Journal: **PHILOSOPHICAL TRANSACTIONS OF THE ROYAL SOCIETY A**

Article id: **RSTA20200263**

Article Title: **Extending the spectral decomposition of Granger causality to include instantaneous influences: application to the control mechanisms of heart rate variability**

First Author: D. Nuzzi

Corr. Author(s): S. Stramaglia

AUTHOR QUERIES – TO BE ANSWERED BY THE CORRESPONDING AUTHOR

As the publishing schedule is strict, please note that this might be the only stage at which you are able to thoroughly review your paper.
Please pay special attention to author names, affiliations and contact details, and figures, tables and their captions.
No changes can be made after publication.

The following queries have arisen during the typesetting of your manuscript. Please answer these queries by marking the required corrections at the appropriate point in the text.

Q1	Please replace [?] with appropriate number.
Q2	While the online version of figures 4 and 5 will be in colour, we have been instructed to print the figures in black and white. Please note that if you have explicitly referred to colour in the caption this may affect the legibility of the figures in print.

PHILOSOPHICAL TRANSACTIONS A

royalsocietypublishing.org/journal/rsta

Research

Cite this article: Nuzzi D, Stramaglia S, Javorka M, Marinazzo D, Porta A, Faes L. 2021 Extending the spectral decomposition of Granger causality to include instantaneous influences: application to the control mechanisms of heart rate variability. *Phil. Trans. R. Soc. A* 20200263. https://doi.org/10.1098/rsta.2020.0263

Accepted: 15 April 2021

One contribution of 17 to a theme issue 'Advanced computation in cardiovascular physiology: new challenges and opportunities'.

Subject Areas:
biomedical engineering, medical physics

Keywords:
causality, spectral analysis, vector autoregression, heart rate variability

Author for correspondence:
S. Stramaglia
e-mail: sebastiano.stramaglia@ba.infn.it

Extending the spectral decomposition of Granger causality to include instantaneous influences: application to the control mechanisms of heart rate variability

D. Nuzzi[1], S. Stramaglia[1], M. Javorka[2], D. Marinazzo[3], A. Porta[4,5] and Luca Faes[6]

[1]Dipartimento Interateneo di Fisica, Universitá degli Studi di Bari Aldo Moro, Bari and INFN, Sezione di Bari, 70126 Bari, Italy
[2]Department of Physiology,Comenius University in Bratislava, Jessenius Faculty of Medicine, 03601 Martin, Slovakia
[3]Department of Data Analysis, Ghent University, 9000 Ghent, Belgium
[4]Department of Biomedical Sciences for Health, University of Milan, Milan, Italy
[5]Department of Cardiothoracic, Vascular Anesthesia and Intensive Care, IRCCS Policlinico San Donato, San Donato Milanese, Milan, Italy
[6]Dipartimento di Ingegneria, Universitá di Palermo, 90128 Palermo, Italy

SS, 0000-0002-5873-8564; AP, 0000-0002-6720-9824; LF, 0000-0002-3271-5348

Assessing Granger causality (GC) intended as the influence, in terms of reduction of variance of surprise, that a driver variable exerts on a given target, requires a suitable treatment of 'instantaneous' effects, i.e. influences due to interactions whose time scale is much faster than the time resolution of the measurements, due to unobserved confounders or insufficient sampling rate that cannot be increased because the mechanism of generation of the variable is inherently slow (e.g. the heartbeat). We exploit a recently proposed framework for the estimation of causal influences in the spectral

THE ROYAL SOCIETY PUBLISHING

domain and include instantaneous interactions in the modelling, thus obtaining (i) a novel index of undirected instantaneous causality and (ii) a novel measure of GC including instantaneous effects. An effective procedure to speed up the optimization of parameters in this frame is also presented. After illustrating the proposed formalism in a theoretical example, we apply it to two datasets of cardiovascular and respiratory time series and compare the values obtained within the frequency bands of physiological interest by the proposed total measure of causality with those derived from the standard GC analysis. We find that the inclusion of instantaneous causality allows to correctly disentangle the baroreflex mechanism from the effects related to cardiorespiratory interactions. Moreover, studying how controlling the respiratory rhythm acts on cardiovascular interactions, we document an increase of the direct (non-baroreflex mediated) influence of respiration on the heart rate in the respiratory frequency band when switching from spontaneous to paced breathing.

This article is part of the theme issue 'Advanced computation in cardiovascular physiology: new challenges and opportunities'.

1. Introduction

The assessment of causal interactions among a set of measured variables, typically performed through the statistical notion of Granger causality (GC) [1], is an important issue in the study of physiological systems, in particular when the interdependencies among different regulatory systems is under investigation [2]. The oscillatory content of physiological systems stimulated the development of methods able to assess GC in the frequency domain [3–5]. This development is fundamental when physiological mechanisms operate at well-known time scales, as is the case for the short-term cardiovascular control where the Mayer waves (of period approx. 10 *s*) and higher frequency rhythms (synchronous with the breathing rate) occur spontaneously as a consequence of the physiological regulation [6].

The model underlying the standard definition of GC is a strictly causal vector autoregressive (VAR) model, which can unambiguously provide causal information only when instantaneous effects are negligible. We remark that the term instantaneous should not be taken literally, as instantaneous influences may be due to interactions whose time scale is much faster than the time resolution of the measurements. Instantaneous influences might be due to unobserved confounders or insufficient sampling rate that cannot be increased because the mechanism of generation of the variable is inherently slow. The latter is the case of the heart and the cardiovascular system, intended as a dynamical systems whose activity is paced by the heartbeat; many of the output variables of these systems, such as the heart period and the systolic arterial pressure (SAP), can be measured once per cardiac beat and thus cannot be assessed at a faster pacing. Such problem often shows up in the analysis of physiological time series [7,8]; a solution to this issue has been proposed in [9] introducing an extended GC measure in the frequency domain that takes into account both lagged and instantaneous influences. A main limitation of this approach is the fact that it assigns a direction to zero-lag effects, and the proposed measure depends on such an assignment. On the other hand, in some cases, a preferential direction for instantaneous influences cannot be assigned *a priori* [10], and more generally instantaneous interactions in VAR models should be un-directed, as discussed in [11].

In this paper, we propose a novel approach to deal with instantaneous interactions in the spectral formulation of GC, which (i) exploits a recently introduced framework [12] that allows one to quantify causal influences in a stochastic dynamical system, both in the time and frequency domains; (ii) introduces a measure of undirected instantaneous causality for multivariate systems; (iii) introduces a measure of extended GC that takes into consideration both lagged and instantaneous causality and does not depend on the direction of instantaneous interactions; (iv) significantly speeds up the evaluation of the model parameters compared to the original proposal [12]. Our approach, differently from [9], does not provide the direction of

the instantaneous interactions among variables; at the same time, no *a priori* knowledge of the instantaneous influences is needed.

The paper is organized as follows. In the next section, we describe the methods, whilst in §3.1, we show the results by the proposed approach on a simulated data set. In §3.2, we turn to consider real data, in particular the application to cardiovascular and cardiorespiratory interactions. Using our measure of GC with instantaneous effects, we can more clearly identify the correct frequency ranges in which each physiological effect is significant, in particular, the activation of the baroreflex mechanism during postural stress and the direct (non-baroreflex mediated) effect of respiration on the RR interval during paced breathing. In §4, we draw some conclusions.

2. Methods

(a) The framework of causal influences in stochastic dynamical systems

In this subsection, we briefly recall a recently introduced framework [12] that quantifies causal influences in a multivariate stochastic dynamical system, both in the time and frequency domains.

Firstly, the system, composed by N subsystems whose activity is mapped by the variables x_1, $\ldots$, x_N, is described using a VAR(p) model (the so-called *full model*), which in principle can account for couplings among every pair of variables

$$\boldsymbol{x}_t = \sum_{k=1}^{p} A_k \boldsymbol{x}_{t-k} + \boldsymbol{\varepsilon}_t, \tag{2.1}$$

where $\boldsymbol{x}_t = [x_{t,1} \ldots, x_{t,N}]^{\mathrm{T}}$ denotes the state of the system at time t, the $N \times N$ matrices A_k contain the coupling coefficients between each process and the regressors, and $\boldsymbol{\varepsilon}_t$ represents normally distributed residuals uncorrelated over time.

Secondly, a *disconnected model* is considered in which some of the influences are cut, i.e. some of the coupling coefficients are forced to zero at all lags

$$\boldsymbol{x}_t = \sum_{k=1}^{p} A'_k \boldsymbol{x}_{t-k} + \boldsymbol{\varepsilon}'_t, \quad \text{where } \forall k = 1, \ldots, p,\ \forall (i,j) \in \Lambda :\ (A'_k)_{ij} = 0. \tag{2.2}$$

The set Λ includes all the combinations of the influences from the time series j to the time series i that are cut; in other words, Λ represents the constraints on the disconnected model; different choices of Λ lead to different types of causal influences that can be assessed in this framework, like GC, integrated information (Φ) and others [12]. Model identification is carried out by minimizing the generalized variance $|\Sigma|$ with respect to the non-zero AR coefficients, where

$$\Sigma = \mathrm{E}[\boldsymbol{\varepsilon}_t \boldsymbol{\varepsilon}_t^{\mathrm{T}}], \tag{2.3}$$

denotes the covariance matrix of the residuals. It can be shown that this procedure, when applied to the full model, is equivalent to the standard generalized least squares (GLS) estimation; the ordinary least squares method (OLS), which minimizes the variance of each residual separately, is less efficient when Σ is not a diagonal matrix and instantaneous correlations are expected. The minimization procedure adopted in [12] is gradient descent, which can be computationally expensive especially in systems with many variables or when an high model order p is needed. We remark that the identification procedure for the disconnected model, given the presence of the constraints Λ, cannot be done using a simple matrix inversion like in the GLS algorithm: this is the reason for an iterative algorithm like the gradient descent.

Given the generalized variances for the full and disconnected model, the causal influence from the series indexed with j to the series indexed with i in the set Λ is defined as [12]

$$CI = \frac{1}{2} \log \left(\frac{|\Sigma'|}{|\Sigma|} \right). \tag{2.4}$$

The measure CI quantifies the increase in the prediction error when some causal links are cut; in [12], it is shown that, for a bivariate system and given a driver variable j and a target variable i, if one chooses the constraints for the disconnected model such that $(A'_k)_{ij} = 0,\ \forall k$ then the resulting causal influence is equivalent to the GC from j to i.

The strength of the formulation of causal influences in [12] is the possibility to give a meaningful spectral decomposition to any causal influence. More specifically, given the spectral density matrices $S(\omega)$ and $S'(\omega)$ obtained from the frequency domain representation of the VAR parameters of the full and disconnected models [2,4,7], the corresponding frequency-domain measure can be computed as

$$ci(\omega) = \frac{1}{2}\log\left(\frac{|S'(\omega)|}{|S(\omega)|}\right). \tag{2.5}$$

It can be proven that $CI = (1/2\pi)\int_{-\pi}^{\pi} ci(\omega)\,\mathrm{d}\omega$, regardless of the choice of the constraints for the disconnected model. Moreover, using the constraints previously discussed to evaluate the GC, the resulting spectral measure is identical to the spectral GC defined by Geweke [3,13].

(b) Including instantaneous interactions in the frame of causal influences

Now we exploit the framework described in the previous Section [12] to deal with GC when instantaneous interactions are not negligible; the formalism here described will be used in following sections. We also show here that this framework allows to estimate the GC in a fast and efficient way solving a set of Yule–Walker equations [14].

We start noting that the presence of instantaneous interaction in a system reflects on the presence of non-zero off-diagonal terms in the covariance matrix of residuals Σ. We remark that the converse is not always true; in other words, the presence of off-diagonal correlations of residuals $\boldsymbol{\epsilon}_t$ does not imply that there are instantaneous interactions between the time series. Moreover, even if the actual instantaneous interactions in the system are directed, the resulting residuals covariance matrix is always symmetric $\Sigma = \Sigma^{\mathrm{T}}$; therefore, the *reconstructed* instantaneous interactions are always bidirectional, see the discussions in [1,11]. In the full model of the time series, we thus include a zero-lag coupling matrix A_0, defining the extended model

$$\boldsymbol{x}_t = \sum_{k=0}^{p} A_k \boldsymbol{x}_{t-k} + \boldsymbol{\varepsilon}_t. \tag{2.6}$$

The matrix A_0 must be chosen so as to have the structure of an acyclic interaction graph: this means that, by a suitable rearrangement of the variables, the non-zero elements of A_0 can be transformed into a strictly triangular matrix with diagonal elements equal to zero [9]. It can be shown that, for any such structure of A_0, fitting the corresponding full model leads to a diagonal covariance matrix of residuals with determinant which does not depend on the structure of A_0 (provided that the structure of A_0 is acyclic).

Given these constraints for the matrix A_0, we now show how to compute the non-zero entries of all the matrices A_k explicitly. First, we compute $\Sigma = \mathrm{E}[\boldsymbol{\varepsilon}_t \boldsymbol{\varepsilon}_t^{\mathrm{T}}]$ using (2.6)

$$\Sigma = \Gamma_0 - \sum_{l=0}^{p} \Gamma_l A_l^{\mathrm{T}} - \sum_{l=0}^{p} A_l \Gamma_l^{\mathrm{T}} + \sum_{l=0}^{p}\sum_{k=0}^{p} A_l \Gamma_{k-l} A_k^{\mathrm{T}}, \tag{2.7}$$

where we denoted the auto-covariance of $\boldsymbol{x}_t$ and $\boldsymbol{x}_{t-k}$ as $\Gamma_k = \mathbb{E}[\boldsymbol{x}_t \boldsymbol{x}_{t-k}^{\mathrm{T}}]$. The optimal components of each A_k can be found as the ones that minimize the generalized variance $|\Sigma|$, as shown in [12]. The minimization procedure can be carried out without Lagrange multipliers, setting to zero the derivatives of $|\Sigma|$ w.r.t. the unconstrained (non-zero) couplings $(A_k)_{ij}$; after some manipulations, it reads

$$\frac{\partial|\Sigma|}{\partial(A_k)_{ij}} = 2|\Sigma|\left[\Sigma^{-1}\left(\sum_{l=0}^{p} A_l \Gamma_{k-l} - \Gamma_k\right)\right]_{ij} = 0, \quad k = 0, \ldots, p. \tag{2.8}$$

The system of equations should be solved, for each $k = 0, \ldots, p$, only for $(i, j) \in \Delta_k$, where $\Delta_k = \{(i, j) \mid (A_k)_{ij} \neq 0\}$ is the set of ordered pairs (i, j) for which the corresponding coupling coefficient is unconstrained at a certain lag k. As an example, when evaluating the full model, if we assume a strictly upper triangular matrix A_0, the constraints would be $\Delta_0 = \{(i, j) | j = 1, \ldots, N \ \wedge \ i < j\}$. The system of equations (2.8) should be solved, in general, using a numeric method like gradient descent. On the other hand, the choice to include the instantaneous matrix A_0 in the model guarantees diagonality of the matrix Σ; in this case, the same is true for its inverse, so that (2.8) reduces to

$$\forall\, k = 0, \ldots, p, \quad \forall (i, j) \in \Delta_k, \quad \left(\sum_{l=0}^{p} A_l \Gamma_{k-l} - \Gamma_k \right)_{ij} = 0. \tag{2.9}$$

We note that the system of equations (2.9) resembles the Yule–Walker equations; this allows it to be readily solved using the algorithm described in the appendix A. It is worth mentioning that the optimization procedure described above might be replaced, for the full model, with more common and simpler methods. On the other hand, the generality of the proposed framework allows us to identify models where some constraints are applied to the entries of the connectivity matrices, as discussed in the following paragraph; such constraints render problematic the use of more common techniques.

We now consider the disconnected model, for which a different set of constraints, denote as ${\Delta_k}'$, determine the zero elements of coupling matrices. Considering the transfer of information from a driver variable j to a target variable i, conditioned on all the other variables in the system, corresponds to set to zero all the lagged couplings from the driver to the target, $({A_k}')_{ij} = 0$ for $k = 1, \ldots, p$, as well as choosing an acyclic structure for the instantaneous matrix ${A_0}'$. It is worth mentioning, at this point, that in the disconnected model not all the acyclic matrices ${A_0}'$ render the covariance of residuals diagonal, differently from what happens for the full model. Therefore, apart from acyclicity, further properties of ${A_0}'$ are required to ensure that Σ' is diagonal. In appendix b, we show how to design the structure of ${A_0}'$ so that Σ' is diagonal, and equation (2.9) hold. Again, one can show that all the acyclic structures of ${A_0}'$ which render the residuals covariance diagonal lead to the same value of the determinant of Σ'.

Then, given the sets of constraints for the full (Δ_k) and disconnected (${\Delta_k}'$) models, both resulting in diagonal covariance matrices Σ and Σ', we use (2.4) to evaluate the conditional GC in the time domain

$$\mathcal{F}_{x_j \to x_i | \boldsymbol{x}_{[i,j]}} = \frac{1}{2} \log \left(\frac{|\Sigma'|}{|\Sigma|} \right), \tag{2.10}$$

where we denoted $\boldsymbol{x}_{[i,j]}$ as the set of conditional variables, i.e. all the variables $\boldsymbol{x} = (x_1, \ldots, x_N)$ excluding x_i and x_j. We remark that the use of the determinant of the full error covariance matrix, instead of the variance of the target variable, allows one to generalize the GC to the multivariate case, as pointed out in [?], and is mandatory when stricter constraints on the VAR model are applied, like in [12]. Furthermore, in order to compute the GC in the frequency domain, we evaluate the transfer function $H(\omega)$ and the spectral density matrix $S(\omega)$ as [2]

$$S(\omega) = H(\omega)\, \Sigma\, H^{\dagger}(\omega), \quad \text{where } H(\omega) = \left(\mathbb{I} - \sum_{k=0}^{p} A_k \, \mathrm{e}^{-\mathrm{i}\omega k} \right)^{-1}, \tag{2.11}$$

and where the superscript † denotes conjugate transpose and $\mathbb{I}$ is the identity matrix. Note that the matrix A_0 must be included in the definition of the transfer function $H(\omega)$ if we want to investigate lagged causality in the presence of instantaneous interactions. The same equations are used to define $H'(\omega)$ and $S'(\omega)$ for the disconnected model, and then the spectral conditional GC can be evaluated as

$$f_{x_j \to x_i | \boldsymbol{x}_{[i,j]}}(\omega) = \frac{1}{2} \log \left(\frac{|S'(\omega)|}{|S(\omega)|} \right). \tag{2.12}$$

We emphasize that (2.10) and (2.12) are exactly equal to the standard definitions of GC in the time and frequency domains given by Granger and Geweke [1–3,14], the main difference being

that in our approach the choice of the driver, target and conditioned variables is simply encoded in the choice of the constraints Δ_k', and that the solution can be computed efficiently using a Yule–Walker-like system of equations (2.9). In the next sections, we will exploit our formalism to introduce a new measure of instantaneous causality.

We conclude this section stressing that in our approach we give up the identifiability of the model, as the instantaneous couplings are not uniquely determined; however, the determinants of the residuals covariance are unique, so the GC estimate is defined unambiguously.

(c) Quantifying instantaneous causality

In this section, we propose a novel measure of instantaneous causality within the framework described in the previous sections. In general, the presence of instantaneous interactions is reflected in non-zero off diagonal entries of the residuals covariance of the VAR model (1). This has lead to define the *instantaneous interaction* measure for a system of two time series as follows [3–5]: calling Σ the covariance matrix, and Σ' a new covariance matrix preserving only the diagonal elements, the log-ratio $ii = \log(|\Sigma'|/|\Sigma|)$ measures the increased uncertainty one gets when neglecting the instantaneous interactions, interpreted as the value of instantaneous causality between the variables.

In the proposed approach, a diagonal residuals covariance Σ is obtained introducing a zero lag matrix A_0 in the model, supposed to correspond to an acyclic structure. To quantify instantaneous causality, we define a disconnected model in which the instantaneous coupling between variables i and j is cut, i.e. $(A_0')_{ij} = (A_0')_{ji} = 0$. This choice introduces non-zero elements in the residuals covariance matrix, $(\Sigma')_{ij} = (\Sigma')_{ji} \neq 0$, and limits us from using (2.9) to solve the disconnected model. As done before, we neglect the newly introduced off-diagonal elements and solve the model using (2.9) anyway, using (2.7) to evaluate the covariance matrix and then discarding the off-diagonal elements. This procedure is justified by the fact that, in this way, we can quantify instantaneous causality as the error in prediction we commit when neglecting one of the instantaneous couplings. Note that our procedure can be carried out in multivariate systems and the corresponding instantaneous causality measure can be conditioned on the other variables in the system. We denote the time domain instantaneous causality measure we get from (2.4) as $\mathcal{F}_{x_i \cdot x_j | \boldsymbol{x}_{[i,j]}}$ and the frequency domain one as $f_{x_i \cdot x_j | \boldsymbol{x}_{[i,j]}}(\omega)$. Note that this measure is symmetrical, i.e. the instantaneous causality from i to j is exactly equal to the instantaneous causality from j to i. Moreover, differently from other instantaneous causality measures in the spectral domain [15], our decomposition is non-negative as required. The spectrum of our definition of instantaneous causality can be proven to be flat, as it has been demonstrated in [12].

(d) Granger causality including instantaneous effects (iGC)

The formalism developed above allows us to introduce, both in the time and frequency domains, a new measure that quantifies the combination of lagged and instantaneous causality. Given a driver variable j and a target variable i in a multivariate system, we introduce a disconnected model in which we combine the lagged and instantaneous constraints that we described in the previous sections. Specifically, we cut all the lagged directional couplings from the driver to the target, $(A_{k>0}')_{ij} = 0$, and we also cut the symmetric instantaneous coupling between them, $(A_0')_{ij} = (A_0')_{ji} = 0$. The remaining constraints on A_0' are identical to the ones given for the GC and are thoroughly discussed in appendix B. The off-diagonal elements that appear in Σ' should be treated like discussed in the previous section. We denote the resulting causality measure as $\mathcal{F}_{x_j \bullet \to x_i | \boldsymbol{x}_{[i,j]}}$ and we call it *Granger causality with instantaneous effects* (iGC); the corresponding frequency domain measure is denoted as $f_{x_j \bullet \to x_i | \boldsymbol{x}_{[i,j]}}(\omega)$. The iGC combines the lagged and the instantaneous causality in a single measure and in our experiments we observed that, in the time domain, it equals the sum of the GC and of the instantaneous causality

$$\mathcal{F}_{x_j \bullet \to x_i | \boldsymbol{x}_{[i,j]}} = \mathcal{F}_{x_j \to x_i | \boldsymbol{x}_{[i,j]}} + \mathcal{F}_{x_i \cdot x_j | \boldsymbol{x}_{[i,j]}}. \tag{2.13}$$

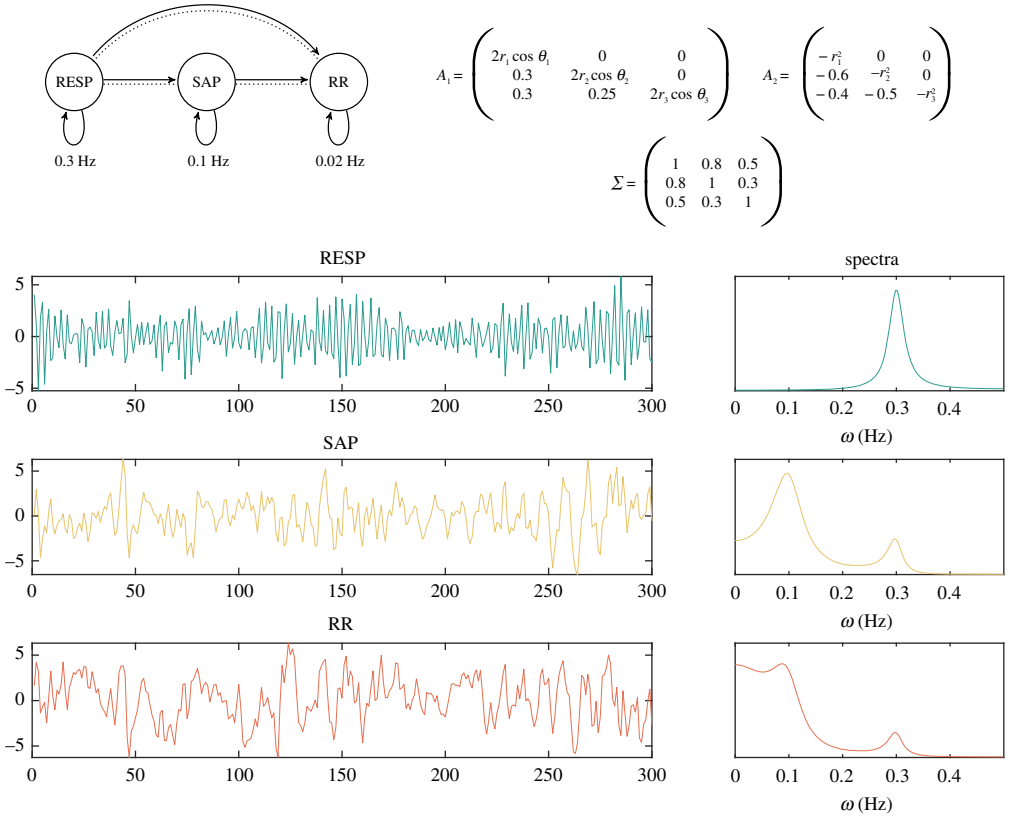

Figure 1. Top left: graph of interactions for the simulated RESP, SAP, RR series. The arrows denotes a lagged coupling or an oscillatory self-interaction at a specified frequency; the dotted lines denote an instantaneous coupling. Top right: the matrices of AR coefficients for the simulated VAR(2) model. The diagonal terms of each matrix are chosen in a way that guarantees an oscillatory behaviour at a desired frequency f_i, where $\theta_i = 2\pi f_i$ (assuming a sampling frequency of 1 Hz) and $r_1 = 0.9$, $r_2 = 0.8$ and $r_3 = 0.55$. Bottom: the first 300 samples of the simulated time series, alongside with the respective spectra. (Online version in colour.)

The same relation does not hold for the corresponding spectral measures. This means that the spectral iGC $f_{x_j \bullet\to x_i|x_{[i,j]}}(\omega)$ is not just a shifted version of the spectral GC and the two may differ significantly. At the same time, the spectrum of the iGC is not flat unless the lagged causality contribution is vanishing. In the next sections, we will analyse simulated and real systems and we will argue that the peaks and valleys of the iGC spectrum can be interpreted in meaningful ways when instantaneous interactions are not negligible.

3. Evaluation on simulated vector autoregressive model

We test the proposed approach on a VAR(2) model producing time series with spectral components similar to those commonly encountered in heart period (RR), systolic pressure (SAP) and respiration (RESP) variability series; the model is similar to those previously used for the same purpose [16,17]. In our simulation, the state of the system at time t is $\boldsymbol{x}_t = (\mathrm{RESP}_t, \mathrm{SAP}_t, \mathrm{RR}_t)$ and we consider both instantaneous and lagged couplings from RESP to SAP, from RESP to RR, and from SAP to RR. The corresponding interaction graph is shown in figure 1, alongside with the matrices A_k. The oscillatory frequencies for the time series are chosen as $f_{\mathrm{RESP}} = 0.3$ Hz, $f_{\mathrm{SAP}} = 0.1$ Hz and $f_{\mathrm{RR}} = 0.02$ Hz, and we assume a sampling frequency of 1 Hz; the presence of instantaneous interaction is encoded in the non-zero off-diagonal elements of the residuals covariance matrix Σ.

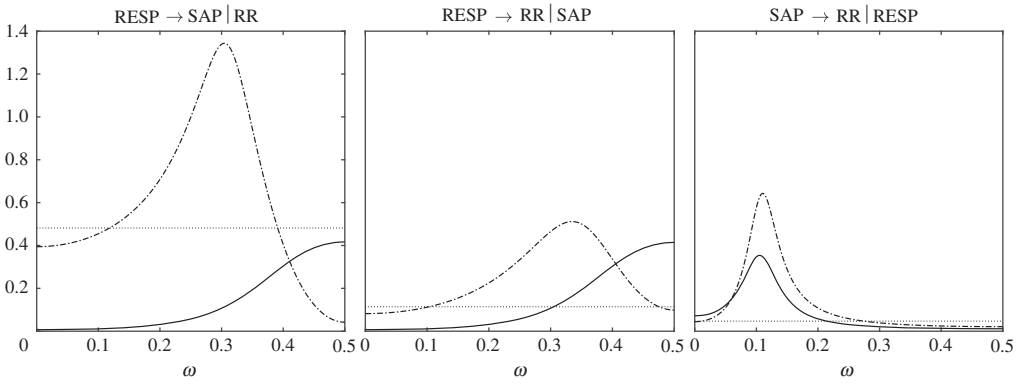

Figure 2. The conditional GC (solid line), instantaneous causality (dotted line) and iGC (dash-dotted line) in the frequency domain for the simulated model, shown only for the directions in which a lagged coupling is present. As discussed, the instantaneous causality has a flat spectrum. Moreover, the area under the iGC curve (the time-domain value of the iGC) is equal to the sum of the areas under the GC curve and the instantaneous causality line. The iGC shows sharp peaks around the frequencies that have a clear interpretation in terms of the physiological rhythms, whilst the standard GC shows a broader spectrum.

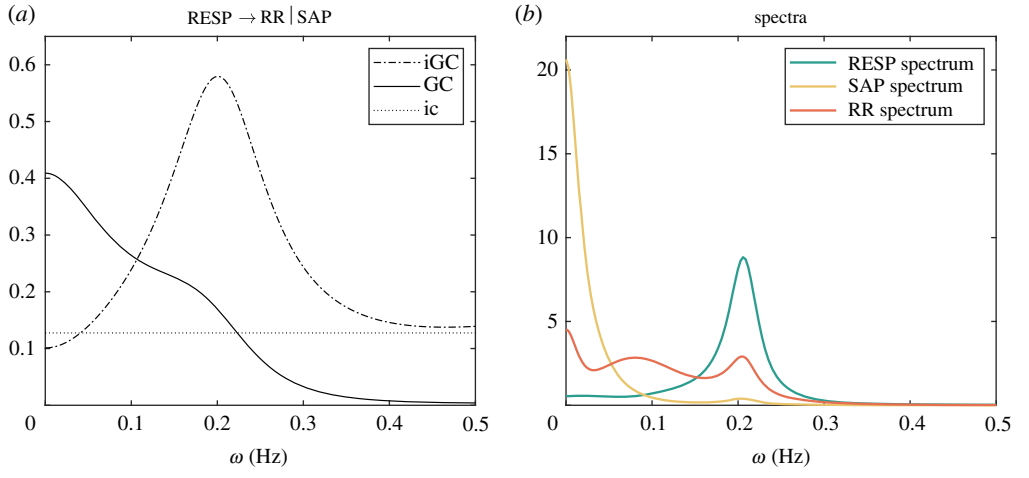

Figure 3. The conditional GC (solid line), instantaneous causality (dotted line) and iGC (dash-dotted line) computed in the frequency domain from RESP to RR conditioned on SAP (*a*), along with the power spectral densities of each series computed from the model coefficients (*b*) for one of the subjects in the HUT dataset that displayed an high contribution of instantaneous effects. The iGC shows a sharper peak around the standard respiratory frequency (approx. 0.2 Hz), an higher contribution at high frequencies and a lower contribution at low frequencies. We remark that the area under the iGC curve is exactly equal to the sum of the areas under the two other curves. (Online version in colour.)

We modelled this connectivity structure because we are interested in assessing the effect of instantaneous interactions on the direct influences from SAP to RR in the absence of any description of the closed-loop RR-SAP relationship. We remark that, while the interactions pattern in this toy model has no closed loops, the application of the proposed framework is not limited to direct acyclic interaction graphs (DAGs) and can be used when feedback loops are present in the system under consideration. We generated one realization of the stationary stochastic process with length $T = 3 \times 10^5$ samples, for which a randomly chosen segment of 300 samples is shown in figure 1 alongside with the corresponding spectra. From the VAR model, we evaluated the correlation matrices Γ_k using the Yule–Walker equations up to the order $q = 100$ and then we used (2.9) to evaluate the matrices A_k' for all the disconnected models.

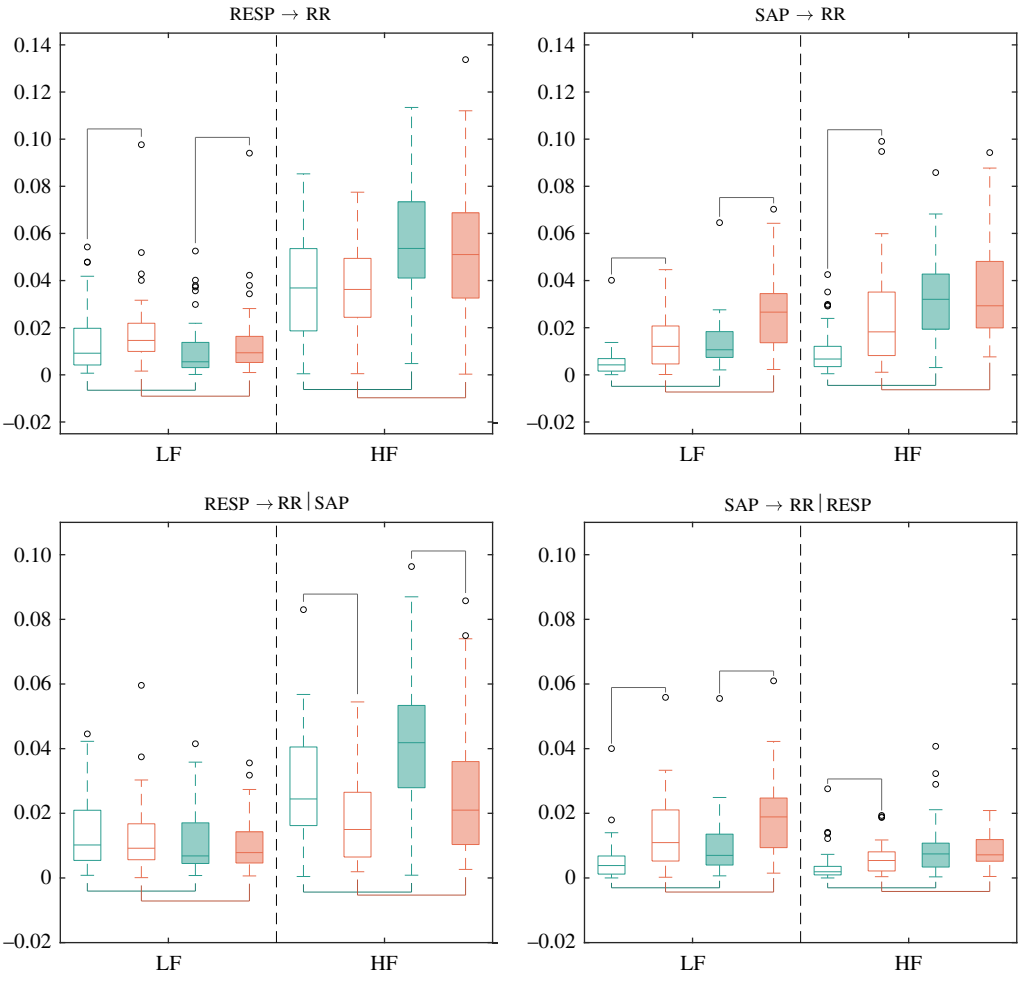

Figure 4. Results of GC analysis for the HUT database. Panels report the boxplot distributions of the pairwise and conditional spectral GC (empty boxes) and iGC (filled boxes) computed in the supine position (green boxes) and in the upright position (orange boxes) integrated over the low frequency (LF, [0.04, 0.15] Hz) and high frequency (HF, [0.15, 0.4] Hz) bands. Lines connecting pairs of distributions denote $p < 0.05$. (Online version in colour.)

The spectral conditional GC, iGC and instantaneous causality are shown in figure 2 for the cases RESP → SAP — RR, RESP → RR — SAP and SAP → RR — RESP. We remark that, as it is clear from the figure, the iGC displays sharp peaks corresponding to frequencies of the driver time series, thus allowing a clear interpretation of causal influences in terms of the underlying physiological rhythms. On the contrary, the standard GC shows a broader spectrum with less interpretable causal influences, especially when the RESP series is taken as the driver.

4. Application to cardiovascular and cardiorespiratory interactions

We analyse two datasets of cardiovascular and respiratory time series previously collected [18,19], which have been already investigated to study cardiovascular and cardiorespiratory interactions through Granger-causal methods during parasympathetic inhibition and sympathetic nervous system activation induced by head-up tilt (HUT) [20] and during the regularizing action of paced breathing (PB) at a rate close to the spontaneous one [17]. The two datasets contain the variability series of consecutive RR intervals measured from the ECG, SAP measured from

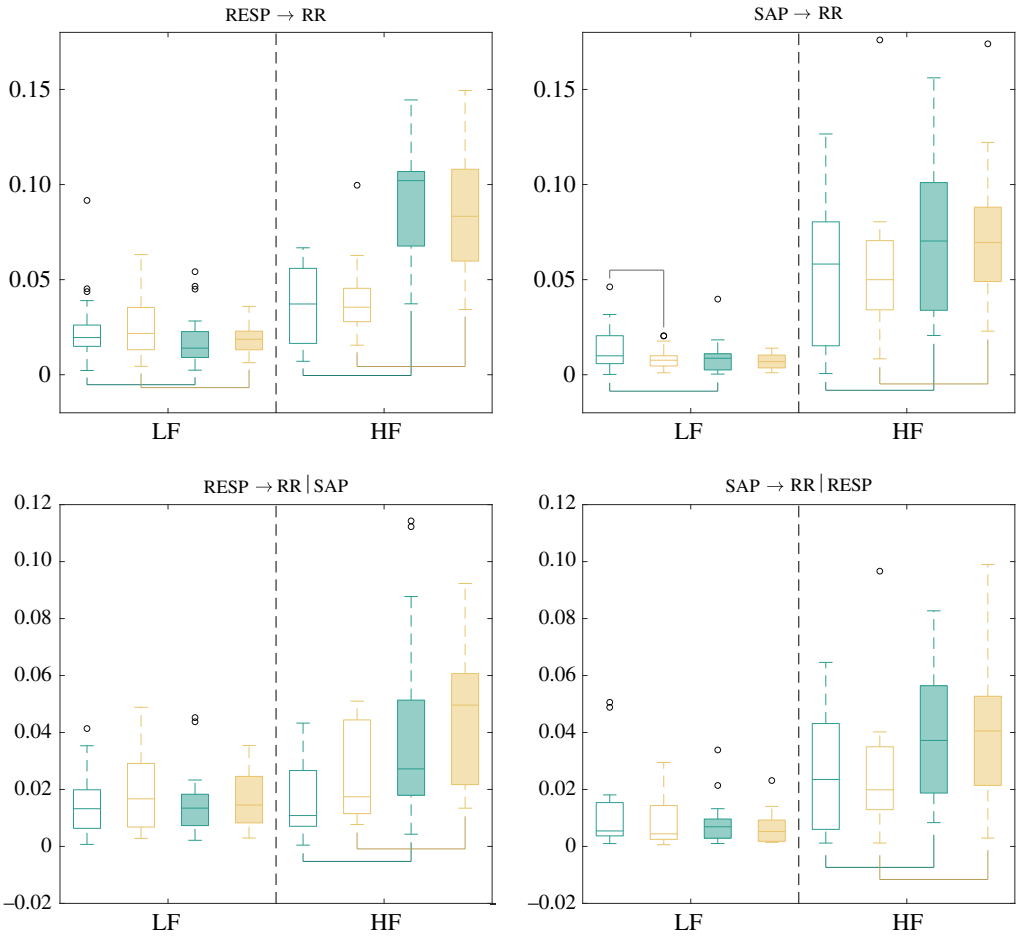

Figure 5. Results of GC analysis for the PB database. Panels report the boxplot distributions of the pairwise and conditional spectral GC (empty boxes) and iGC (filled boxes) computed during spontaneous breathing (green boxes) and during paced breathing (yellow boxes) integrated over the low frequency (LF, [0.04, 0.15] Hz) and high frequency (HF, [0.15, 0.4] Hz) bands. Lines connecting pairs of distributions denote $p < 0.05$. (Online version in colour.)

the arterial pressure signal recorded non-invasively through the volume-clamp method, and respiration signal (RESP, measured via inductive plethysmography in the HUT database and via a nasal thermistor in the PB database). The HUT database consisted of time series lasting 300 heartbeats collected in the resting supine position and in the upright position (45 degrees) from 61 healthy young volunteers (37 female, 17.5 ± 2.4 yrs). The PB database consisted of time-series lasting 256 heartbeats collected during spontaneous breathing in the resting position and during controlled breathing at 15 breaths/min from 19 healthy young volunteers (11 female, 27–35 yrs). Both protocols adhered to the principles of the Declaration of Helsinki, and were approved by the ethical committee of the Jessenius Faculty of Medicine, Comenius University, Martin, Slovakia (HUT protocol) and by the ethical review board of the 'L. Sacco' Hospital and of the Department of Technologies for Health of the University of Milan, Italy (PB protocol).

In both databases, the adopted measurement convention is that the nth SAP value is contained within the nth RR interval, and the nth RESP value is sampled at the onset of the nth RR interval. The VAR model identification was performed for each set of time series using the least squares method, setting the model order according to the Akaike information criterion [21] for each subject, resulting in model orders between 3 and 5. Given the model coefficients, the correlation

Table 1. Statistical analysis for the first database; comparison supine versus upright position.

	LF		HF	
GC	*p*-value	Kendall *W*	*p*-value	Kendall *W*
RESP → RR	0.016	0.061	0.843	0
SAP → RR	<0.001	0.293	<0.001	0.168
RESP → RR | SAP	0.252	0.007	0.002	0.097
SAP → RR | RESP	<0.001	0.497	<0.001	0.293
	LF		HF	
iGC	*p*-value	Kendall *W*	*p*-value	Kendall *W*
RESP → RR	0.012	0.142	0.255	0.013
SAP → RR	<0.001	0.329	0.403	0.006
RESP → RR | SAP	0.320	0.033	<0.001	0.168
SAP → RR | RESP	<0.001	0.368	0.462	0

matrices Γ_k were evaluated using the Yule–Walker equations up to the order $q = 100$ for all sets of series. Then, from the Γ_k matrices, we evaluated all the matrices A_k and A_k' for the full and disconnected models using (2.9) and, consequently, all the GC, iGC and instantaneous causality from RESP and SAP to RR, both in time and frequency domain. As an example, in figure 3, we show the spectral GC, iGC and instantaneous causality, from RESP to RR conditioned on SAP, for one of the subjects in the dataset that showed an high contribution of instantaneous effects. The iGC exhibits a sharper peak around the respiratory frequency compared to the standard GC and, at the same time, it shows a lower contribution at lower frequencies.

To perform group analysis, we integrated each spectral causality measure in the two frequency bands of physiological interest: the LF band ($[0.04, 0.15]$ Hz) and the HF band ($[0.15, 0.4]$ Hz) [22]. Results for the two datasets are illustrated in figures 4 and 5, respectively, depicting the distribution across subjects of the GC and the iGC, assessed separately for the two frequency bands in both the analysed conditions. In each case, statistically significant differences between the two conditions or between the GC and the iGC are shown as lines connecting the relevant pairs of distributions. The statistical comparisons between the two conditions and between the two methods is carried out using the Wilcoxon signed-rank test; a significance level $\alpha = 0.05$ was chosen for both tests. Moreover, the corresponding effect sizes were calculated using the Kendall's W parameter. The results of the comparison between the two phases are shown in table 1 (HUT) and table 3 (PB), while the comparison between the two methods is shown in table 2 (HUT) and table 4 (PB).

The analysis of the HUT database (figure 4 and tables 1 and 2) reveals that, in the LF band, Q2 the information transfer from SAP to RR increases significantly moving from the supine to the upright body position. This results, which holds both for the GC and the iGC, and for pairwise and conditional measures, is expected as it reflects the well-known activation of the baroreflex mechanism as a response to the postural stress whereby LF pressure oscillations are more effectively transmitted to the heart rate [17,20]. In general, we find that, regardless of the body position, including instantaneous causality increases the LF values of the information transfer from SAP to RR and decreases the LF values of the information transfer from RESP to RR. These results document the importance and appropriateness of considering instantaneous causality in the analysis of cardiovascular interactions, where zero-lag effects are expected to contribute significantly to the baroreflex mechanism [9,16], and of cardiorespiratory interactions, where negligible information transfer is expected to occur from RESP to RR in the LF band [23]. In the HF band, a significant increase of the GC SAP → RR and SAP → RR | RESP with the transition from the supine to the upright position is observed only if we neglect instantaneous causality;

Table 2. Statistical analysis for the first database; comparison GC versus iGC.

	LF		HF	
supine	*p*-value	Kendall *W*	*p*-value	Kendall *W*
RESP → RR	<0.001	0.284	<0.001	0.934
SAP → RR	<0.001	0.640	<0.001	0.871
RESP → RR | SAP	<0.001	0.218	<0.001	0.640
SAP → RR | RESP	<0.001	0.538	<0.001	0.640
	LF		HF	
upright	*p*-value	Kendall *W*	*p*-value	Kendall *W*
RESP → RR	<0.001	0.444	<0.001	0.640
SAP → RR	<0.001	0.871	<0.001	0.250
RESP → RR | SAP	0.002	0.09	<0.001	0.401
SAP → RR | RESP	<0.001	0.640	<0.001	0.09

Table 3. Statistical analysis for the second database; comparison spontaneous versus paced breathing.

	LF		HF	
GC	*p*-value	Kendall *W*	*p*-value	Kendall *W*
RESP → RR	0.520	0.003	1	0.025
SAP → RR	0.027	0.224	0.687	0.003
RESP → RR | SAP	0.243	0.136	0.070	0.335
SAP → RR | RESP	0.070	0.136	0.260	0.136
	LF		HF	
iGC	*p*-value	Kendall *W*	*p*-value	Kendall *W*
RESP → RR	0.748	0.003	0.295	0.069
SAP → RR	0.573	0.003	0.904	0.025
RESP → RR | SAP	0.778	0.003	0.445	0.069
SAP → RR | RESP	0.159	0.025	0.520	0.003

this suggests that baroreflex activation resulting in a stronger transfer of information from SAP to RR is actually active only in the LF band [8], while finding it in the HF band seems indicative of inappropriate modelling of the instantaneous effects. On the other hand, RESP → RR | SAP decreases significantly from rest to tilt in the HF band, which has been previously documented and reflects a weakening of the non-baroreflex respiratory sinus arrhythmia mechanisms during postural stress [24]. Finally, we find that the inclusion of instantaneous causality increases the HF values for all the measures. This fact, that was previously observed for cardiorespiratory interactions assessed during postural stress [9], can be explained if we consider the instantaneous effects as fast (within-sample) contributions to the dynamics of the system.

The analysis of the PB database (figure 5 and tables 3 and 4) shows that LF values are small or negligible for all measures. This confirms the lack of respiratory sinus arrhythmia effects in the LF band seen before when RESP is the driver [23], and indicates that—contrary to the postural stress - the paced breathing manoeuver does not elicit changes in the baroreflex involvement [24]. In the HF band, all measures are significantly higher when computed considering instantaneous effects, confirming in the PB protocol the results obtained for the HUT protocol and the

Table 4. Statistical analysis for the second database; comparison GC versus iGC

	LF		HF	
spontaneous	*p*-value	Kendall *W*	*p*-value	Kendall *W*
RESP → RR	0.006	0.136	<0.001	1
SAP → RR	0.004	0.468	<0.001	0.623
RESP → RR | SAP	0.748	0.025	<0.001	1
SAP → RR | RESP	0.064	0.335	<0.001	0.8
	LF		HF	
paced	*p*-value	Kendall *W*	*p*-value	Kendall *W*
RESP → RR	0.01	0.136	<0.001	1
SAP → RR	0.243	0.003	<0.001	0.468
RESP → RR | SAP	0.084	0.069	<0.001	0.8
SAP → RR | RESP	0.159	0.069	<0.001	0.8

importance to account for within-beat interactions in the analysis of faster cardiovascular and cardiorespiratory effects [9,25]. Variations from spontaneous to paced breathing are small; these findings agree with those reported previously using time-domain measures information transfer [17,24], and confirm the general observation that paced breathing does not alter significantly the cardiovascular autonomic regulation compared with spontaneous breathing [26]. Nevertheless, the increase of the conditional GC RESP → RR—SAP in the HF band supports the hypothesis that non-baroreflex (mostly central) mechanisms of respiratory sinus arrhythmia may be enhanced by controlling the respiratory rhythm.

5. Conclusion

The construction of methodologies for the estimation of instantaneous causality is an important problem as it is connected with the problem of assessing the total causality that a variable exerts on a given target. In this paper, we have coped with this issue exploiting a new framework for the estimation of causal influences in the spectral domain [12] and by including instantaneous effects in the modelling approach pursued by this framework. Our approach assumes undirected instantaneous interactions, eliminating the need to set the directionality of instantaneous couplings through the exploitation of prior knowledge or the involvement of cumbersome non-Gaussian modelling which characterized previous approaches [9,10]. This leads us to propose a novel index of undirected instantaneous causality, whose spectrum is flat, that generalizes the measure of instantaneous influence to multivariate systems. Consequently, we introduced a measure of GC including instantaneous effects, the iGC, that is consistently equal to the sum of the GC and the instantaneous causality in the time domain but, at the same time, has a spectral version which may differ significantly from the standard spectral GC defined by Geweke [3,13]). This highlights the importance of the proposed frequency decomposition, as demonstrated by the results shown for the simulation and real data examples. Moreover, we introduce a procedure to speed up the optimization of parameters w.r.t. the original proposal in [12].

We applied the proposed formalism to two datasets of cardiovascular and respiratory time series and compared the values obtained by the new total measure of causality with those from the standard GC. In cardiovascular variability analysis, instantaneous interactions typically occur as within-beat effects between the observed time series (e.g. the heart period, arterial pressure and respiration) which likely result from common driving factors such as the neuro-autonomic regulation. Therefore, it is important to account for instantaneous effects in the

analysis of GC between cardiovascular time series, also in view of the fact that GC quantifies the causal effect that the underlying mechanism (in this case, autonomic control) has on the measured variables, rather than quantifying the mechanism itself [?]. In other words, data-driven methods to infer statistical dependencies always come with this ambiguity of confusing map and territory, and methods used to compute them with target properties of the system under exam [?]. Our results show that the spectral iGC, differently from the standard GC, peaked more clearly at the physiologically relevant frequencies when instantaneous effects were significant. For the first dataset, investigating the effects of postural stress on cardiovascular and cardiorespiratory interactions, we observed that the inclusion of instantaneous causality allowed us to correctly identify expected effects on the baroreflex control of the heart rate and on cardiorespiratory interactions. In particular, we observed that, when considering instantaneous causality, the influence of SAP on the RR intervals increases at low frequencies and that the non-baroreflex influence of the respiration on RR decreases in the high-frequency range. Moreover, we observed that, while the standard GC would suggest a significant increase at all frequencies of the baroreflex activation mechanism when switching from the supine to the upright body position through head-up tilt, the iGC shows that the increase is only significant in the LF band. The analysis of the second dataset, describing the effects of paced breathing on cardiovascular interactions, showed that the iGC more clearly identifies the lack of respiratory sinus arrhythmia effects in the LF band, represented by small or negligible value of the iGC and, at the same time, it confirms an increase of the direct (non-baroreflex) effect of respiration on the RR in the HF band when switching from spontaneous to paced breathing.

Future studies are envisaged to compare directly the patterns of time and frequency-domain causality between cardiovascular and respiratory variability provided by the present framework and previous works modelling directed instantaneous effects [9,10], as well as to explore the potential of the GC measures proposed here in contexts where instantaneous effects are known to impact significantly on causality analysis; the latter issue is typical in the study of brain connectivity, e.g. in functional magnetic resonance imaging where the acquired signal represents a smoothed hemodynamic response and is severely undersampled [27–29] and in electroencephalography where the volume conduction effect is a main confounding source of zero-lag correlations [30,31].

Data accessibility. This article has no additional data.

Authors' contributions. Idea: L.F. Supervision: L.F., S.S. and D.M. Experiments and data collecting: M.J. and A.P. developed the algorithm and wrote the code, made the analysis and figures: D.N. All the authors contributed to the discussions and the writing of the manuscript.

Competing interests. We declare we have no competing interests.

Funding. No funding has been received for this article.

Appendix A

Given the set of $(p+1)$ correlation matrices Γ_k, each of size $N \times N$, we want to solve the system of equations

$$\forall\, k = 0, \ldots, p, \quad \forall (i,j) \in \Delta_k, \quad \left(\sum_{l=0}^{p} A_l \Gamma_{k-l} - \Gamma_k \right)_{i,j} = 0 \tag{A 1}$$

for the unknowns $(A_k)_{i,j}$, where $\Delta_k = \{(i,j) \mid (A_k)_{i,j} \neq 0\}$ is the set of unconstrained auto-regressive coefficients for each k. First, we introduce the matrices

$$A = \begin{pmatrix} A_0 & A_1 & \ldots & A_p \end{pmatrix}, \qquad \Gamma = \begin{pmatrix} \Gamma_0 & \Gamma_1 & \ldots & \Gamma_p \end{pmatrix}, \qquad \Psi = \begin{pmatrix} \Gamma_0 & \Gamma_1 & \ldots & \Gamma_p \\ \Gamma_1^{\mathrm{T}} & \Gamma_0 & \ldots & \Gamma_{p-1} \\ \vdots & \vdots & \ddots & \vdots \\ \Gamma_p^{\mathrm{T}} & \Gamma_{p-1}^{\mathrm{T}} & \ldots & \Gamma_0 \end{pmatrix}, \tag{A 2}$$

and then, if we make the matrix product explicit, we can rewrite (A 1) as

$$\sum_{l=0}^{p}\sum_{r=1}^{N}(A_l)_{i,r}(\Gamma_{k-l})_{r,j}-(\Gamma_k)_{i,j}=\sum_{l=0}^{p}\sum_{r=1}^{N}(A)_{i,(l+1)r}(\Psi)_{(l+1)r,(k+1)j}-(\Gamma)_{i,(k+1)j}=0, \tag{A 3}$$

where the same restrictions on the indices (i, j) as (A 1) should be applied. We now want to replace the column index $(k+1)j$, but in order to do that we need to rewrite the constraints in a different way. First, we fix the row index i and define the set

$$\Omega_i=\left\{n\in\mathbb{N}\;\middle|\;\exists j,k:(i,j)\in\Delta_k\ \wedge\ n=(k+1)j\right\}, \tag{A 4}$$

then we can write

$$\forall\, i=1,\ldots,N,\quad \forall\, n\in\Omega_i,\quad \sum_{m=1}^{(p+1)N}(A)_{i,m}(\Psi)_{m,n}-(\Gamma)_{i,n}=0, \tag{A 5}$$

where the summations over l and r have been replaced by the summation over $m=(l+1)r$. We note that for $m\notin\Omega_i$ the corresponding term in the sum vanishes, so we can write $\sum_{m=1}^{(p+1)N}\rightarrow\sum_{m\in\Omega_i}$. The fact that we are only considering $m, n\in\Omega_i$ suggests that we may consider the new matrices $\hat{A}_i$, $\hat{\Gamma}_i$, $\hat{\Psi}_i$ where the rows/columns corresponding to indices not in Ω_i are removed and rewrite the previous equation as

$$\hat{A}_i\hat{\Psi}_i-\hat{\Gamma}_i=0, \tag{A 6}$$

which can be readily solved by matrix inversion $\hat{A}_i=\hat{\Gamma}_i\hat{\Psi}_i^{-1}$. The elements in the row vector $\hat{A}_i$ can then be remapped to corresponding non-zero values of $(A_k)_{i,j}$. We can informally say that we are solving the Yule–Walker equations row-by-row and that, for each row, we are removing all the columns corresponding to couplings that should be forced to zero.

Appendix B

In this section, we show how to ensure a diagonal Σ' matrix for the disconnected model when evaluating conditional GCs in a multivariate system. We denote the target variable index as τ. First, we observe that each component of the matrix can written as

$$(\Sigma')_{ij}=\left(\Gamma_0-\sum_{l=0}^{p}A'_l\Gamma_l^{\mathrm{T}}\right)_{ij}-\sum_{a\neq j}\left(\Gamma_0-\sum_{l=0}^{p}A'_l\Gamma_l^{\mathrm{T}}\right)_{ia}(A'_0)_{ja}-\sum_{a\neq j}\sum_{k=1}^{p}\left(\Gamma_k-\sum_{l=0}^{p}A'_l\Gamma_{k-l}\right)_{ia}(A'_k)_{ja}. \tag{B 1}$$

The Yule–Walker-like terms can be set to zero using (2.9) if they correspond to an unconstrained coupling coefficient and, at the same time, we can use the instantaneous matrix $A_0{}'$ to cancel the last two terms in the equation. We note that, given the fact that Σ' is a symmetric matrix, we need only to force half of the elements to zero. In particular, we set $\Sigma_{ij}=0$ for $j>i$, $i\neq\tau$ and at the same time $\Sigma_{i\tau}=0$ for $i>\tau$. This choice ensures that all the off-diagonal elements are vanishing and, at the same time, that the row index i is never equal to the target index τ. This allows us to simplify the last term in (B 1) using (2.9), knowing that for $i\neq\tau$ the coupling coefficients $(A_k{}')_{ia}$ are unconstrained. The two equations for the components of Σ' can now be written as

$$\left.\begin{aligned}\forall\, i\neq\tau,\forall\, j>i,\quad (\Sigma')_{ij}&=\left(\Gamma_0-\sum_{l=0}^{p}A'_l\Gamma_l^{\mathrm{T}}\right)_{ij}-\sum_{a\neq j}\left(\Gamma_0-\sum_{l=0}^{p}A'_l\Gamma_l^{\mathrm{T}}\right)_{ia}(A'_0)_{ja},\\ \forall\, i>\tau,\quad (\Sigma')_{i\tau}&=\left(\Gamma_0-\sum_{l=0}^{p}A'_l\Gamma_l^{\mathrm{T}}\right)_{i\tau}-\sum_{a\neq\tau}\left(\Gamma_0-\sum_{l=0}^{p}A'_l\Gamma_l^{\mathrm{T}}\right)_{ia}(A'_0)_{\tau a}.\end{aligned}\right\} \tag{B 2}$$

The remaining terms can be cancelled if we correctly identify the instantaneous effects matrix $A_0{}'$. Our choice, that in general is not the only possible one, can be described as follows: we

consider a strictly upper triangular matrix and then we transpose the τ-th row. This ensures that each component in the system can instantaneously affect each other while keeping the row of the target variable empty. This choice can be written as

$$\begin{cases} \forall\, i \geq j, & (A_0')_{ij} = 0 \\ \forall\, j > \tau, & (A_0')_{\tau j} = 0 \\ \forall\, i \neq \tau,\ \forall\, j > i, & (A_0')_{ij} = \times \Rightarrow \left(\Gamma_0 - \sum_{l=0}^{p} A_l' \Gamma_l^{\mathrm{T}} \right)_{ij} = 0 \\ \forall\, i > \tau, & (A_0')_{i\tau} = \times \Rightarrow \left(\Gamma_0 - \sum_{l=0}^{p} A_l' \Gamma_l^{\mathrm{T}} \right)_{i\tau} = 0, \end{cases} \tag{B 3}$$

where we denoted with $\times$ the unconstrained entries of the matrix. First, we note that the third and fourth equation on the right side of (B 3) allows us to simplify the first term in both equations in (B 2). Then, splitting the remaining summations like

$$\left.\begin{aligned} &\forall\, i \neq \tau, \forall\, j > i, \quad (\Sigma')_{ij} = -\sum_{a<j} \left(\Gamma_0 - \sum_{l=0}^{p} A_l' \Gamma_l^{\mathrm{T}} \right)_{ia} (A_0')_{ja} - \sum_{a>j} \left(\Gamma_0 - \sum_{l=0}^{p} A_l' \Gamma_l^{\mathrm{T}} \right)_{ia} (A_0')_{ja}, \\ &\forall\, i > \tau, \quad (\Sigma')_{i\tau} = -\sum_{a<\tau} \left(\Gamma_0 - \sum_{l=0}^{p} A_l' \Gamma_l^{\mathrm{T}} \right)_{ia} (A_0')_{\tau a} - \sum_{a>\tau} \left(\Gamma_0 - \sum_{l=0}^{p} A_l' \Gamma_l^{\mathrm{T}} \right)_{ia} (A_0')_{\tau a}. \end{aligned}\right\} \tag{B 4}$$

we can use the first two equations in (B 3) to simplify the first term in the first equation and both the terms in the second one and, at the same time, use the third equation in (B 3) to simplify the remaining term. We have shown that our choice for $A_0{}'$ always guarantees a diagonal covariance matrix Σ' when we only consider the lagged causality, i.e. the GC. If we want to evaluate the iGC the additional constraints on $A_0{}'$ we simply add the additional constraints to the ones described in (B 3). We note that the constraints on $A_0{}'$ that guarantee a diagonal Σ' do not depend on the choice of the driver variable. This allows us to generalize the previous argument to the case of many drivers and to evaluate multivariate GC and iGC.

References

1. Granger CW. 1969 Investigating causal relations by econometric models and cross-spectral methods. *Econometrica* **37**, 424–438. (doi:10.2307/1912791)
2. Porta A, Faes L. 2015 Wiener–Granger causality in network physiology with applications to cardiovascular control and neuroscience. *Proc. IEEE* **104**, 282–309. (doi:10.1109/JPROC.2015.2476824)
3. Geweke J. 1982 Measurement of linear dependence and feedback between multiple time series. *J. Am. Stat. Assoc.* **77**, 304–313. (doi:10.1080/01621459.1982.10477803)
4. Ding M, Chen Y, Bressler S 2006 *Granger causality: basic theory and application to neuroscience*. Handbook of Time Series Analysis. Wienheim: Wiley.
5. Cohen D, Tsuchiya N. 2018 The effect of common signals on power, coherence and Granger causality: theoretical review, simulations, and empirical analysis of fruit fly LFPs data. *Front. Syst. Neurosci.* **12**, 30. (doi:10.3389/fnsys.2018.00030)
6. Cohen MA, Taylor JA. 2002 Short-term cardiovascular oscillations in man: measuring and modelling the physiologies. *J. Physiol.* **542**, 669–683. (doi:10.1113/jphysiol.2002.017483)
7. Baselli G, Porta A, Rimoldi O, Pagani M, Cerutti S. 1997 Spectral decomposition in multichannel recordings based on multivariate parametric identification. *IEEE Trans. Biomed. Eng.* **44**, 1092–1101. (doi:10.1109/10.641336)
8. Javorka M, Czippelova B, Turianikova Z, Lazarova Z, Tonhajzerova I, Faes L. 2017 Causal analysis of short-term cardiovascular variability: state-dependent contribution

of feedback and feedforward mechanisms. *Med. Biol. Eng. Comput.* **55**, 179–190. (doi:10.1007/s11517-016-1492-y)
9. Faes L, Erla S, Porta A, Nollo G. 2013 A framework for assessing frequency domain causality in physiological time series with instantaneous effects. *Phil. Trans. R. Soc. A* **371**, 20110618. (doi:10.1098/rsta.2011.0618)
10. Schiatti L, Nollo G, Rossato G, Faes L. 2015 Extended Granger causality: a new tool to identify the structure of physiological networks. *Physiol. Meas.* **36**, 827. (doi:10.1088/0967-3334/36/4/827)
11. Kirchgässner G, Wolters J, Hassler U. 2013 Granger causality. In *Introduction to Modern Time Series Analysis*, pp. 95–125. New York, NY: Springer.
12. Cohen D, Sasai S, Tsuchiya N, Oizumi M. 2020 A general spectral decomposition of causal influences applied to integrated information. *J. Neurosci. Methods* **330**, 108443. (doi:10.1016/j.jneumeth.2019.108443)
13. Geweke JF. 1984 Measures of conditional linear dependence and feedback between time series. *J. Am. Stat. Assoc.* **79**, 907–915. (doi:10.1080/01621459.1984.10477110)
14. Barnett L, Seth AK. 2014 The MVGC multivariate Granger causality toolbox: a new approach to Granger-causal inference. *J. Neurosci. Methods* **223**, 50–68. (doi:10.1016/j.jneumeth.2013.10.018)
15. Chicharro D. 2011 On the spectral formulation of Granger causality. *Biol. Cybern* **105**, 331–347. (doi:10.1007/s00422-011-0469-z)
16. Faes L, Marinazzo D, Montalto A, Nollo G. 2014 Lag-specific transfer entropy as a tool to assess cardiovascular and cardiorespiratory information transfer. *IEEE Trans. Biomed. Eng.* **61**, 2556–2568. (doi:10.1109/TBME.2014.2323131)
17. Faes L, Porta A, Nollo G. 2015 Information decomposition in bivariate systems: theory and application to cardiorespiratory dynamics. *Entropy* **17**, 277–303. (doi:10.3390/e17010277)
18. Javorka M *et al.* 2018 Towards understanding the complexity of cardiovascular oscillations: insights from information theory. *Comput. Biol. Med.* **98**, 48–57. (doi:10.1016/j.compbiomed.2018.05.007)
19. Porta A, Bassani T, Bari V, Pinna GD, Maestri R, Guzzetti S. 2011 Accounting for respiration is necessary to reliably infer Granger causality from cardiovascular variability series. *IEEE Trans. Biomed. Eng.* **59**, 832–841. (doi:10.1109/TBME.2011.2180379)
20. Faes L, Porta A, Nollo G, Javorka M. 2017 Information decomposition in multivariate systems: definitions, implementation and application to cardiovascular networks. *Entropy* **19**, 5. (doi:10.3390/e19010005)
21. Akaike H. 1974 A new look at the statistical model identification. *IEEE Trans. Autom. Control* **19**, 716–723. (doi:10.1109/TAC.1974.1100705)
22. Berntson GG *et al.* 1997 Heart rate variability: origins, methods, and interpretive caveats. *Psychophysiology* **34**, 623–648. (doi:10.1111/j.1469-8986.1997.tb02140.x)
23. Saul JP, Berger RD, Albrecht P, Stein S, Chen MH, Cohen R. 1991 Transfer function analysis of the circulation: unique insights into cardiovascular regulation. *Am. J. Physiol. Heart Circ. Physiol.* **261**, H1231–H1245. (doi:10.1152/ajpheart.1991.261.4.H1231)
24. Faes L, Nollo G, Porta A. 2011 Information domain approach to the investigation of cardio-vascular, cardio-pulmonary, and vasculo-pulmonary causal couplings. *Front. Physiol.* **2**, 80. (doi:10.3389/fphys.2011.00080)
25. Faes L, Nollo G, Porta A. 2013 Compensated transfer entropy as a tool for reliably estimating information transfer in physiological time series. *Entropy* **15**, 198–219. (doi:10.3390/e15010198)
26. Pinna GD, Maestri R, La Rovere MT, Gobbi E, Fanfulla F. 2006 Effect of paced breathing on ventilatory and cardiovascular variability parameters during short-term investigations of autonomic function. *Am. J. Physiol. Heart Circ. Physiol.* **290**, H424–H433. (doi:10.1152/ajpheart.00438.2005)
27. Deshpande G, Sathian K, Hu X. 2010 Assessing and compensating for zero-lag correlation effects in time-lagged Granger causality analysis of fMRI. *IEEE Trans. Biomed. Eng.* **57**, 1446–1456. (doi:10.1109/TBME.2009.2037808)
28. Wu G, Liao W, Stramaglia S, Ding J, Chen H, Marinazzo D. 2013 A blind deconvolution approach to recover effective connectivity brain networks from resting state fMRI data. *Med. Image Anal.* **17**, 365. (doi:10.1016/j.media.2013.01.003)

29. Diez I *et al.* 2015 Information flow between resting-state networks. *Brain Connectivity* **5**, 554. (doi:10.1089/brain.2014.0337)
30. Van de Steen F, Faes L, Karahan E, Songsiri J, Valdes-Sosa PA, Marinazzo D. 2019 Critical comments on EEG sensor space dynamical connectivity analysis. *Brain Topogr.* **32**, 643–654. (doi:10.1007/s10548-016-0538-7)
31. Kotiuchyi I, Pernice R, Popov A, Faes L, Kharytonov V. 2020 A framework to assess the information dynamics of source EEG activity and its application to epileptic brain networks. *Brain Sci.* **10**, 657. (doi:10.3390/brainsci10090657)